

# Lab on a Chip

Accepted Manuscript



This is an *Accepted Manuscript*, which has been through the Royal Society of Chemistry peer review process and has been accepted for publication.

*Accepted Manuscripts* are published online shortly after acceptance, before technical editing, formatting and proof reading. Using this free service, authors can make their results available to the community, in citable form, before we publish the edited article. We will replace this *Accepted Manuscript* with the edited and formatted *Advance Article* as soon as it is available.

You can find more information about *Accepted Manuscripts* in the [Information for Authors](#).

Please note that technical editing may introduce minor changes to the text and/or graphics, which may alter content. The journal's standard [Terms & Conditions](#) and the [Ethical guidelines](#) still apply. In no event shall the Royal Society of Chemistry be held responsible for any errors or omissions in this *Accepted Manuscript* or any consequences arising from the use of any information it contains.



# Lab on a Chip

## PAPER

### Microfluidic co-culture platform to quantify chemotaxis of primary stem cells

Z. Tatárová,<sup>a</sup> J.P. Abbuehl,<sup>a</sup> S. Maerkl,<sup>b</sup> and J. Huelsken<sup>a</sup>

Received 00th January 20xx,  
Accepted 00th January 20xx

DOI: 10.1039/x0xx00000x

[www.rsc.org/](http://www.rsc.org/)

Functional analysis of primary tissue-specific stem cells is hampered by their rarity. Here we describe a greatly miniaturized microfluidic device for the multiplexed, quantitative analysis of the chemotactic properties of primary, bone marrow-derived mesenchymal stem cells (MSC). The device was integrated within a fully customized platform that both increased the viability of stem cells *ex vivo* and simplified manipulation during multidimensional acquisition. Since primary stem cells can be isolated only in limited number, we optimized the design for efficient cell trapping from low volume and low concentration cell suspensions. Using nanoliter volumes and automated microfluidic controls for pulsed medium supply, our platform is able to create stable gradients of chemoattractant secreted from mammalian producer cells within the device, as was visualized by a secreted NeonGreen fluorescent reporter. The design was functionally validated by a CXCL/CXCR ligand/receptor combination resulting in preferential migration of primary, non-passaged MSC. Stable gradient formation prolonged assay duration and resulted in enhanced response rates for slowly migrating stem cells. Time-lapse video microscopy facilitated determining a number of migratory properties based on single cell analysis. Jackknife-resampling revealed that our assay requires only 120 cells to obtain statistically significant results, enabling new approaches in the research on rare primary stem cells. Compartmentalization of the device not only facilitated such quantitative measurements but will also permit future, high-throughput functional screens.

#### Introduction

Adult tissue specific stem cells are recognized as an essential cellular reservoir in many physiological and pathological processes such as tissue homeostasis, repair, aging and cancer. These stem cells are rare and typically account for only 0.005 to 3% of cells in any tissue.<sup>1-3</sup> New technologies are urgently required that would allow functional studies with this important cell population.<sup>4-6</sup> The characterization of primary stem cells is, however, greatly impaired by their low number and their rapid phenotypic alteration upon extraction from the body. *In vitro* passaging is known to alter important cellular functions and markers.<sup>7</sup> Thus only the *ex vivo* use of primary cells can ensure phenotypic and genetic integrity. The low number of cells which can be isolated for such *ex vivo* studies limits the types of assays which can be performed resulting in an only fragmentary understanding of primary stem cell biology.

One important aspect of stem cells is their activation in response to tissue damage in order to assist the wound healing

process. This involves attraction of stem cells by soluble cues to sites of injury.<sup>8</sup> Chemotaxis describes the ability of cells to sense a gradient of extracellular factor across its cell body by differential, localized activation of corresponding receptors. Next, the signal is amplified and translated into adjustments of the cytoskeletal architecture for directional migration along the gradient.<sup>9</sup> The study of chemotaxis typically uses devices such as the Boyden chamber.<sup>10</sup> With the recent development of a 96-well Boyden chamber format (ChemoTx®System) even high-throughput studies are possible. However, a large number of cells (~10000) are required for a single measurement which makes this method incompatible with rare cells. Additionally, the produced gradients lack temporal stability resulting in a low frequency of responding cells. To overcome these limitations, researchers moved towards microfluidic platforms to further miniaturize the assay and to form stable gradients for extended assay duration. Combining chip-based assays with automated time-lapse microscopy allows evaluation of the chemotaxis process at the single cell level.<sup>11</sup> These microfluidic devices further permit combining multiple cell types over physiologically relevant distances and time-scales.<sup>12</sup> However until now, these designs have not been adapted to rare, primary stem cells and instead used established cell lines.<sup>13</sup> Moreover, relatively large culturing chambers were implemented which precludes efficient trapping of small cell populations and limits the throughput of these platforms.<sup>14-16</sup> Importantly, current designs evaluated trapping efficiency by quantification of the occupancy of traps

<sup>a</sup> École Polytechnique Fédérale de Lausanne (EPFL), ISREC (Swiss Institute for Experimental Cancer Research), Lausanne CH-1015, Switzerland.

<sup>b</sup> École Polytechnique Fédérale de Lausanne (EPFL), STI (School of Engineering) and IBI (Interfaculty Institute of Bioengineering), Lausanne CH-1015, Switzerland.

† Footnotes relating to the title and/or authors should appear here.

Electronic Supplementary Information (ESI) available: [details of any supplementary information available should be included here]. See DOI: 10.1039/x0xx00000x

instead of optimizing the number of trapped cells relative to the input as it is required for rare cells.<sup>17-20</sup>

Here we developed a greatly miniaturized in vitro culturing platform for phenotypic characterization of primary stem cells. We focused on chemotaxis of mesenchymal stem cells (MSC) since these cells are actively recruited to the sites of injury where they affect wound healing responses or to tumor sites where they can support cancer progression.<sup>21</sup> The mechanisms of recruitment of MSC and the involved chemoattractants are, however, still largely unknown. We developed a new chemotaxis platform that combines efficient trapping of rare cells, paralleled assays for repeated measurements, and co-culture of responder and producer cells for on-chip production of chemoattractants by mammalian cells. Our platform permits generating significant, quantitative results from very few, primary stem cells, and will help identifying new chemoattractants of these cells. The device can easily be scaled up for future screening purposes. To our knowledge we are the first to perform chemotaxis analysis with primary stem cells.

## Materials and methods

### Fabrication of the microfluidic device

We used multilayer soft lithography to fabricate two-layered microfluidic devices with integrated, pressure-controlled valves for fluid flow manipulation. The design including flow and control layers was 12.3 mm by 44.8 mm (**Supplementary Fig. 1**) and was done in CleWin 4 (Phoenix Software). The designs were exposed on transparencies at 20000 dpi (Heidelberg DWL200, Heidelberg Instruments Mikrotechnik, Germany). The pattern of channels for the control layer was produced with SU-8 GM1070 (Gersteltec, Switzerland) on silicon wafers. For the flow layer we used AZ-9620 (AZ Electronic Materials, Germany). To promote complete valve closure in the assembled devices, the channel profiles were rounded on the flow layer mold by placing the wafer on a hotplate at 110 - 120 °C for 25 s. Twenty-one baking conditions were tested to find an optimum for this photoresist reflow that did not destroy the trapping structures (**Supplementary Fig. 1**). For the flow layer, 31.5 g of PDMS (20 : 1; polymer : catalyst) was mixed, degassed, poured over a Trimethylchlorosilane (TMCS, Sigma) treated silicon wafer and spun at 1500 rpm. The PDMS was then cured for 30 min at 80 °C. The first ten PDMS replicates were routinely discarded due to toxicity of TMCS for mammalian cells (**Supplementary Table 1**). For the control layer, 42 g of PDMS (5 : 1; polymer : catalyst) was mixed, degassed and poured over a TMCS treated silicon wafer and cured for 30 min at 80 °C. After punching the inlet holes for the control layer, the two layers were aligned and bonded for 2 h at 80 °C. Inlet holes were then punched on the flow layer and the assembly was bonded to a 50 x 70 mm<sup>2</sup> glass slide for 12 h at 80 °C.

### Cell culture

We used primary bone marrow derived mesenchymal stem cells isolated from actin-GFP FVB mice. One mouse was used for each on-chip experiment. Briefly, 4-10 week old FVB mice were sacrificed by CO<sub>2</sub> and their femurs were cleaned from muscles and fascia. The bones were crushed gently in a mortar and cells of the bone matrix were released by incubation in 1 ml of a 3% collagenase solution (C0130, Sigma) in a shaker at 37 °C for 45 min. The cells were collected and filtered with a 100 µm strainer (BD Falcon) and resuspended in 2% fetal bovine serum (FBS). This bone marrow stromal cell preparation was further purified from immune, endothelial and erythrocyte populations by magnetic-activated cell sorting (MACS) depletion. Briefly, cells were labelled with CD45-biotin (30-F11, eBioscience), CD31-biotin (MEC13.3), CD11b-biotin (M1/70) and Ter119-biotin (BioLegend) in 2% FBS for 30 min on ice. After washing, cells were resuspended into MACS Buffer (PBS, 0.5% BSA, 2mM EDTA) and incubated with anti-biotin microbeads (Miltenyi Biotec). After 20 min at 4 °C, the sample was rinsed and resuspended at 10<sup>8</sup> cells/mL. This lineage depletion was performed with an AutoMACS Pro (Miltenyi Biotec). The purified mesenchymal stem cells (MSCs) were cultured in high-glucose DMEM (31 966, Gibco) supplemented with 9% FBS (10 270, Gibco), 9% horse serum (SH30074.03, Hyclone) and 1% penicillin/streptomycin (15 070, Gibco). Cells were plated on collagen-coated cell culture dishes (TPP), and cultured at 37 °C and 7.5% CO<sub>2</sub>, 1% O<sub>2</sub>. The MSC identity was verified by the tri-lineage differentiation potential into adipocytes, chondrocytes and osteocytes (data not shown).

In order to produce CXCR3 expressing MSCs, third generation lentiviral vectors were used. The vector contained two promoters (CMV + PGK, oriented in different directions) for simultaneous expression of a marker (NLS-mCherry) which was used to track the infected cells. Briefly, lentiviral production was done in HEK293T cells at 70% confluence. Transfection of lentiviral backbone, helper and packaging plasmids used standard calcium-phosphate DNA precipitates and virus was harvested after 2 days. MSCs at day 2 of culture were transduced with the lentiviral vector and used for on-chip experiments on day 6. Similarly, CXCR3 expressing human HEK293T (R3) cells and murine L-cells expressing CXCL10 were produced. Cells infected with the vector backbone constructs served as controls (named wt). In this case, high-expressing clones were selected by fluorescent cytometry. The secNeonGreen<sup>22</sup> cDNA was produced by PCR on a construct listed under GenBank KC295282 using the following primers: gcgTTTAAAgccgccaccatgggagtgcaaggtctgtttgcctgatctgcatgctgtggccgaggccgactacaaagacgaggatgcccggcaccatggtgagcaagggcgaggga and tcaTCTAGAttactaagatcttccggactatagagctcgtccatgcc which introduced a Gaussia signal sequence at the N-terminus. secNeonGreen<sup>+</sup> HEK293T cells were prepared by transfection of the NeonGreen expression vector together with a linearized puromycin resistance vector at a 2:1 ratio and selected with puromycin (1 µg/ml) starting 48 h after transfection for at least 7 days. These HEK293T cells were sorted by flow cytometry for

the highest expressing cells at passage 5 after puromycin selection.

#### Automated chip control and cell culture system

Our on-chip valves were actuated via external solenoid valves (VQ110-5F, SMC, USA) that were managed through a custom Beanshell script within the MicroManager 1.4 software (<https://www.micro-manager.org>) controlling the imaging setup. The valves were controlled by a custom-made USB device using a PIC18F2550 microprocessor, a 74HC373 bus system and ULN2003 Darlington drivers. Pneumatic regulators that provide pressurized air to the on-chip valves and the fluid bottles were an AR40N04B (7.5 to 123 psi, SMC) for the control layer and a high-precision low pressure regulator (0.5 to 2 psi, R230-020E, Parker) for the flow layer, respectively. Loading the cells into the closed device with only 0.5 - 1 psi pressure increased the viability of the cells (**Supplementary Table 1**).

The microfluidic device was introduced into a custom-made incubation holder (**Fig. 1b**) which allows submerging the device and exposing the bottom glass plate of the chip directly to the microscope objective. The holder is composed of three main pieces: a lower stainless steel plate, a PEEK frame and an acrylic glass top lid. (i) The metal plate with the outer dimensions of a universal-sample holder sits firmly in the microscope stage to prevent displacements during imaging. The glass slide with the microfluidic device is fixed between the metal plate and the (ii) central frame which also contains a supply inlet for CO<sub>2</sub> and a digital Pt100 resistance thermometer (SMT16030) for temperature measurements in close proximity to the microfluidic device. (iii) The top lid contains a lowered, central glass slide which is below buffer level in the fully assembled device to prevent formation of air bubbles and water condensation which would interfere with the light path. A gas layer is created around this central part which allows efficient gas exchange between the buffer and the CO<sub>2</sub> controlled gas atmosphere inside the holder. Silicon foam on the sides of the lid hold in place the thin tygon tubes connected to the chip without compromising their patency. This way the moving stage does not perturb the microfluidic system while acquiring images at multiple positions. Four screws are used to sandwich the elements listed above in order to ensure the mechanical integrity and prevent buffer leakages. Thin silicon foam tubes are inserted in between the elements for perfect sealing.

For life-imaging microscopy, an incubator box with temperature control by heated air (Cube, Live Imaging Services) surrounds the microscope to keep the temperature constant at 37 °C. Inside the holder, the PDMS device is covered with a bicarbonate buffer: 44mM NaHCO<sub>3</sub>, pH 7.5 in normal air (0.04% CO<sub>2</sub>). For pH control of the microfluidic device, this buffer is kept in a 7.5% CO<sub>2</sub> atmosphere (CO2Mix20, Wave Biotech, USA) resulting in pH 7.4. PDMS is highly gas and water vapour permeable which ensures gas exchange between the buffer and the culture medium inside the cell culture chambers of the device.<sup>23</sup> The system allows

long-term culturing and imaging of cells on-chip and we have used it for up to 7days of culture and time-lapse recording.

#### Image acquisition, processing and data analysis

For image acquisition, an Olympus IX81 automated inverted microscope with multi-channel fluorescence imaging was used, equipped with a high power white LED light source (Sola light) for long-term fluorescent imaging, a 20x objective with correction collar (Olympus UCPLFLN 20x/0,7) to compensate for the thickness of the glass slide of the microfluidics chip and a 10x objective (Zeiss, AchroStigmat 10x/0.25), a computer-controlled, motorized x/y stage (SCAN IM 120 x 80, Märzhäuser) and a high sensitivity USB camera (Retiga 6000, QImaging). The stage, image acquisition and the pressure valves were all controlled in combination via MicroManager 1.4 run on a Supermicro X8DAH server with two Xeon E5630 4 core processors, a GeForce GTX480 card graphics card, 72Gb RAM and 10Tb storage. Imaging was performed automatically every 15 - 60 min by first capturing a bright field image (10 ms exposure), followed by the mCherry channel (1.5 s) and the GFP channel (1 s). The images were stored as Tagged Image File Format (TIFF) files.

Fluorescence signal quantification was performed with ImageJ.<sup>24</sup> To determine the number of fluorescent cells, manual thresholding and background noise reduction with the median filter algorithm was used, followed by segmentation using the classic Watershed algorithm (<http://bigwww.epfl.ch/sage/soft/watershed>) and the cell number was counted using the "Analyze Particle" plugin in ImageJ with a minimal nucleus size of 2.5µm diameter. If watershed processing was not able to segment clusters of cells, the average size of a cell was used to estimate the cell number based on the total fluorescent area. All numerical calculations were performed in MATLAB (MathWorks).

For chemotaxis quantification, the nuclear mCherry signal was used to define cell positions using ImageJ as defined above. Centroid positions were measured relative to the starting point of the migration channel. These distances were recorded at 3, 6, 9 and 12 hours or at 5, 10, 15 and 20h for HEK cells and primary MSC, respectively. The number of cells in the control (wt) or the experimental migration channel (CXCL10) was normalized to the total number of loaded cells. Results of 10 units (**Fig. 1d**) were averaged and used to determine the ratio of migrating cells. The average Y displacement was calculated by accumulating all migrated distances of individual cells per side per unit which was normalized by the total number of migrating cells per unit. Again, results of 10 units were averaged and used to calculate statistical significance. Jackknife resampling (delete-m observations) was performed in Perl by recalculating t-test statistics (paired samples and one-tailed distribution) after progressively removing individual units. The reported p values are the average of p values of all possible combinations of m units out of the initial 10 units.

### Pulsed supply, on-chip protein production and gradient formation as analysed by fluorescence

In order to visualize protein secretion and gradient formation on-chip, secNeonGreen<sup>+</sup> HEK cells were loaded into the producer chambers on one side and wt control cells on the other side. Only after the cells had adhered (1 h), we supplemented them with fresh culture medium. Automated cycles of “pulsed supply” contained periods of medium flow in the side channels which were alternated with flow-free periods for medium replacement by diffusion: (i) new medium was flown through side channels for 30 min while the side valves were closed; (ii) afterwards, medium flow was stopped with valves at the inlet and outlet followed by opening the side valves for 30 min resulting in replenishing the producer chambers with fresh medium by diffusion. We abbreviate this cycle 30/30 (30 min flow / 30 min medium replacement). Valves between the individual producer or responder chambers were closed permanently. Temporally separating medium flow and medium exchange prevented flow of liquid across the unit resulting in generation of stable concentration differences in the two migration channels on opposing sides of the responder chamber. In experiments measuring protein production on-chip, no cells were loaded to the responder chamber. Protein concentrations were measured by fluorescent intensity of secreted NeonGreen protein. Fluorescent images were acquired using a 20x objective and 700ms exposure in the GFP channel always at the 22<sup>nd</sup> minute of the flow step. Gradients were quantified by measuring the fluorescent intensity across the migration channel. The data was normalized to the background and the noise was removed by moving average filtering (window size 10  $\mu\text{m}$ ). We do not show data from the valve areas since these interfere with the fluorescence intensity measurements. In order to evaluate the temporal stability and uniformity of the system, the average absolute fluorescent intensity was measured in a 60x250 $\mu\text{m}$  area at distance of 250 $\mu\text{m}$  from the responder chamber in both migration channels and either these or their difference were reported. Relative variation of these measurements was calculated by dividing their standard deviation with their mean. The average relative variation between units (spatial stability of the effect) was calculated using the average of each hourly time point per unit for 20hours. The average relative variation over time (temporal stability of the effect) was calculated using the results from 10 units per time point. All numerical processing was done in MATLAB.

### Protocol for chemotaxis of mammalian cells on chip

To set up a device, we first sterilized the holder and tubing with 70% EtOH followed by air drying in a sterile laminar flow and washes with sterile water (**Supplementary Table 1**). We next connected the device to the solenoid valves via distilled water filled TYGON tubing (Cole Palmer, USA). The pressure to the control layer was then slowly increased to 35 psi and correct valve closure was validated visually. Afterwards, the flow layer was connected and coated directly with a 100  $\mu\text{g}/\text{ml}$  bovine collagen I solution (PureCol, Advanced BioMatrix, USA)

in HBSS. In order to remove air from the chip, outlet valves were closed while the solution was kept at 2 psi for 45 min at RT. Subsequently the inlet valves were closed and the device was incubated for 45 min at 37 °C inside the microscope incubator. The flow layer was then washed with filtered (0.22 $\mu\text{m}$ , Biofil) PBS before seeding the producer cells into the device (**Supplementary Fig. 3a-c**).

In order to prepare the cells, (i) debris in the cell suspension was removed by filtering through 100 $\mu\text{m}$  cell strainers (Falcon) and centrifugation at 340  $xg$  for 5 min. (ii) Loading medium containing 5 - 20% FBS was filtered (0.22 $\mu\text{m}$ ) and kept at room temperature. (iii) Producer cells were loaded at 1.5 psi (5.4  $\mu\text{l}/\text{min}$  volumetric speed) for up to 2 min. After loading (**Supplementary Fig. 3d**) the producer cells, the device was submerged under the bicarbonate buffer and the holder was assembled.

For chemotaxis experiments, control wt and experimental L10 producer cells were loaded at ~1000 cells/chamber in culture medium with 20% FBS. The cells were cultured with closed valves until they adhered (3.5 h) followed by pulsed supply with the inner side valves closed using 60/30 cycles (**Supplementary Fig. 3e**). Responder cells were loaded 11 h after the producer cells into the central chamber at 0.5 - 1 psi (2.2 - 3.4  $\mu\text{l}/\text{min}$  volumetric speed; **Supplementary Fig. 3f**). Stable cell lines (R3 HEK) were loaded as 20 - 40% cell suspension (50000 - 100000 cells/ $\mu\text{l}$ ) and primary MSCs at 1000 - 2000 cells/ $\mu\text{l}$  for up to 2 min. A total of 5-10  $\mu\text{l}$  of the cell suspension was used for loading. Seeding of the cells in the responder chambers was controlled visually and the loading was stopped when the distribution along all 10 units was equal. After loading, the responders were allowed to adhere and co-culture was started by opening the inner side valve ~1 h after loading using medium with 10% FBS (**Supplementary Fig. 3g**). During the chemotaxis assay, cells were supplied by pulsed supply of 35/5 cycles. The assays were stopped at 12 h for HEK293T or at 20 h for primary MSC, since MSC migrate slower than HEK cells. To refresh the medium for the responder cells during the longer MSC assay the chip was perfused through the central responder chambers after 10 hours. Using a pressure of 0.8psi for 1 min replenished the central volume ~50 times and did not move the mesenchymal stem cells from their original positions. Responder chambers and migration channels were imaged every 15 - 30 min.

## Results

### Design of the microfluidic platform for the analysis of primary stem cell chemotaxis

For assessing cell chemotaxis of primary mesenchymal stem cells, we aimed for developing a novel platform that fulfils the following criteria: (i) long-term culture of primary stem cells in a microfluidic device, (ii) efficient capture of a rare cell population, (iii) on-chip production of chemoattractants with high biological activity by mammalian cells<sup>25</sup>, (iv) generating temporally and spatially stable concentration gradients and (v)

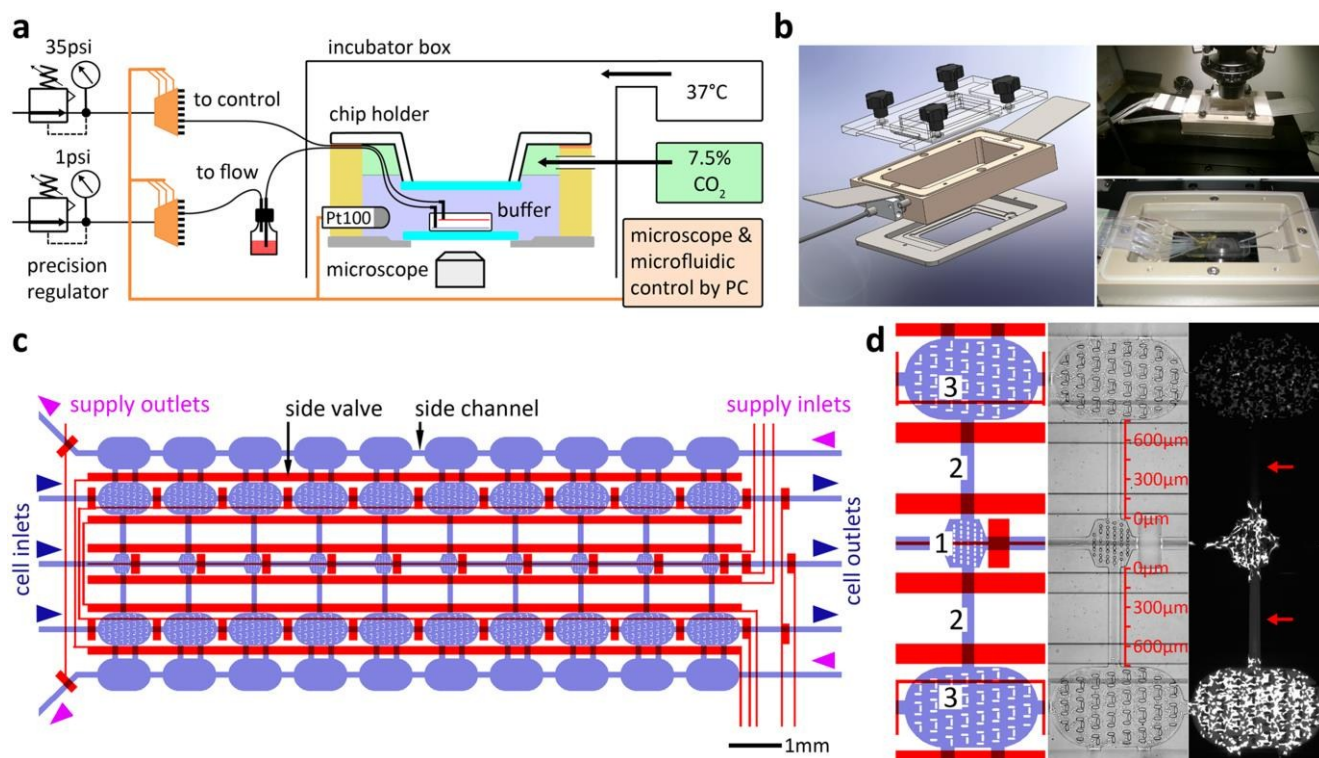


**Fig. 1** Microfluidic platform for chemotaxis assays of primary stem cells. **(a)** Schematic presentation of the experimental setup with factors increasing the viability of primary mesenchymal stem cells (from left to right): Precise pressure regulator (0.5-2 psi) reduced shear forces during loading of cells. The device was assembled in a custom-made holder and is submerged in a carbonate buffer under CO<sub>2</sub>-controlled atmosphere. Temperature is controlled in the incubator box surrounding the microscope. **(b)** Design of the holder (left) and pictures of the submerged microfluidic device in the holder mounted on the motorized stage of the inverted microscope. A fully assembled holder (top right) and a holder without the top lid are displayed (bottom right). **(c, d)** Design of the co-culture chemotaxis device compartmentalized into 10 identical basic units (c): each basic unit (d, left) contained a central responder chamber (1) for efficient trapping of rare stem cells. On both sides, migration channels (2) connect to producer chambers (3) with cells releasing chemoattractants. Bright field (middle; with scale) and fluorescent (right) images of primary GFP<sup>+</sup> MSCs (mid) in co-culture with GFP<sup>+</sup> control (top) and secNeonGreen<sup>+</sup> (bottom) producer cells. The secretion of secNeonGreen created a concentration difference (red arrows) in the migration channels on the opposing sides of the responder chamber 3h after the start of the co-culture.

characterization and quantification of cell migration by video microscopy.

Primary stem cells are known to be very sensitive to ex vivo conditions,<sup>26</sup> and initially MSC did not survive overnight culture in a closed, microfluidic device (**Supplementary Fig. 4a**). Thus we applied a series of optimizations that helped to improve the viability of primary MSC on chip (**Supplementary Table 1** and **Supplementary Fig. 4**). Long-term culture of cells was achieved by precisely controlling osmolarity, pH, temperature and exchange of the cell culture medium. To this end, a special microfluidic chip holder (**Fig. 1a, b**) was constructed which allowed submerging the microfluidic device. Since PDMS is highly water vapour permeable, this maintained osmolarity of the culture medium in the device by preventing evaporation (cf.<sup>23</sup>). A Pt100 resistance thermometer incorporated into the holder measured the temperature in close proximity to the microfluidic device, while temperature regulation was achieved by using an incubator box and a precision air heater. This maintained the temperature of the device at 37°C for growing cells and enhanced focus stability since the whole microscope was kept at a constant temperature. An additional advantage of this holder is that it is mounted firmly to the automated microscope preventing

misalignment, fixes the supply tubing to avoid loosening connections and thereby allows unattended operation for several days while providing time-lapse images. Loading the cells with a precise pressure regulator (0.5 - 1.5 psi, volumetric speed 2.2 - 5.4 µl/min) was another factor that increased cell viability (**Fig. 1a** and **Supplementary Table 1**).

We used multilayer soft lithography to fabricate a poly(dimethylsiloxane) (PDMS) device for quantitative chemotaxis analysis of rare cell population (**Fig. 1c, d**). The chemotaxis assay region was composed of 10 units with a height of 28µm (**Fig. 1c**). This height allowed unrestricted loading of mammalian cells which have a diameter of about 10 - 15 µm in suspension. Five fluid inputs were available: two side supply inlets for the culture medium and three cell inlets for loading of up to three different cell types. The supply and cell inlets were located on opposing sides of the assay region. Each unit included one central “responder chamber” (320 x 360 µm, **Fig. 1d**: ①) of hexagonal shape which contained pillars for efficient entrapment of a low density cell population. On each side of this chamber, migration channels (740 x 100µm, **Fig. 1d**: ②) connected to ellipsoid-shaped “producer chambers” (980 x 600µm; with trapping structures similar to<sup>27</sup>, **Fig. 1d**: ③). Side channels with reservoirs that served to

supply the cells with fresh culture medium copied the shape of the producer chambers but lacked trapping structures. Cells in the central responder chamber were co-cultured with cells in the outer producer chambers. In a typical experiment, one of the producer chambers contained cells engineered to secrete a certain chemotactic factor (experimental side) while the second producer chamber contained parental control cells (control side). As a consequence, the secretome of the producer cells was as similar as possible on both sides except for the target chemoattractant. This arrangement ensured that cells in the central responder chamber were exposed specifically to concentration differences of the chemoattractant. Cells expressing the corresponding chemokine receptor should respond to this concentration difference with preferential movement into the experimental migration channel. In the current form with 10 multiplexed units, the chip already provided the possibility to use replicates for statistical analysis. In the future, the system can easily be adapted for larger screening studies by increasing the number of units and using on-chip transfection of the producer cells with a spotted cDNA expression library.

The design of the responder chamber was optimized to trap a maximal number of cells from a diluted cell suspension, since only  $\sim 10^4$  primary mesenchymal stem cells can be isolated from one mouse, and manipulation requires a minimal loading volume of 5  $\mu\text{L}$ . We tested a number of designs which differed in a central, kite-shape pillar which was included to localize the cells in close proximity to the openings of the migrations channels. However, these designs did not trap a sufficient number of cells and were discarded (Fig. 2a). Instead, the final iteration used a hexagonal chamber with compact trapping structures of ellipsoid shape (25 or 33  $\mu\text{m}$  long and 20  $\mu\text{m}$  wide, Fig. 2a and Supplementary Figure 1). An asymmetrical offset (4 - 12  $\mu\text{m}$ ) of rows was introduced because this was previously shown to improve overall entrapment when compared to symmetrically offset rows.<sup>28</sup> We used two different sizes of gaps (4 and 6  $\mu\text{m}$  width) between neighbouring pillars since the size of primary MSC in suspension is heterogeneous (between 9 - 15  $\mu\text{m}$ ). The biggest gap of 14  $\mu\text{m}$  was designed to leave space for cell passage to downstream chambers. This arrangement of trapping pillars resulted in equal loading within the chamber and over all basic units (Fig. 2a - c and Supplementary Figure 5), and was used for all subsequent experiments including the final chemotaxis setup. Loading primary MSC at concentrations of 1000 or 2000 cells/ $\mu\text{L}$  resulted in homogenous entrapment of  $\sim 40$  or  $\sim 80$  cells per chamber, respectively (Fig. 2c, Supplementary Fig. 5). Since we were limited in the number of MSC we could extract, we were interested to determine the efficiency of cell loading which we calculated by comparing the total number of cells loaded into the assay region with the total number of cells trapped in all 10 units. The overall trapping efficiency of our design was about 20%; we noted that further increasing or reducing the loading concentration resulted in either low trapping efficiency or unequal trapping.

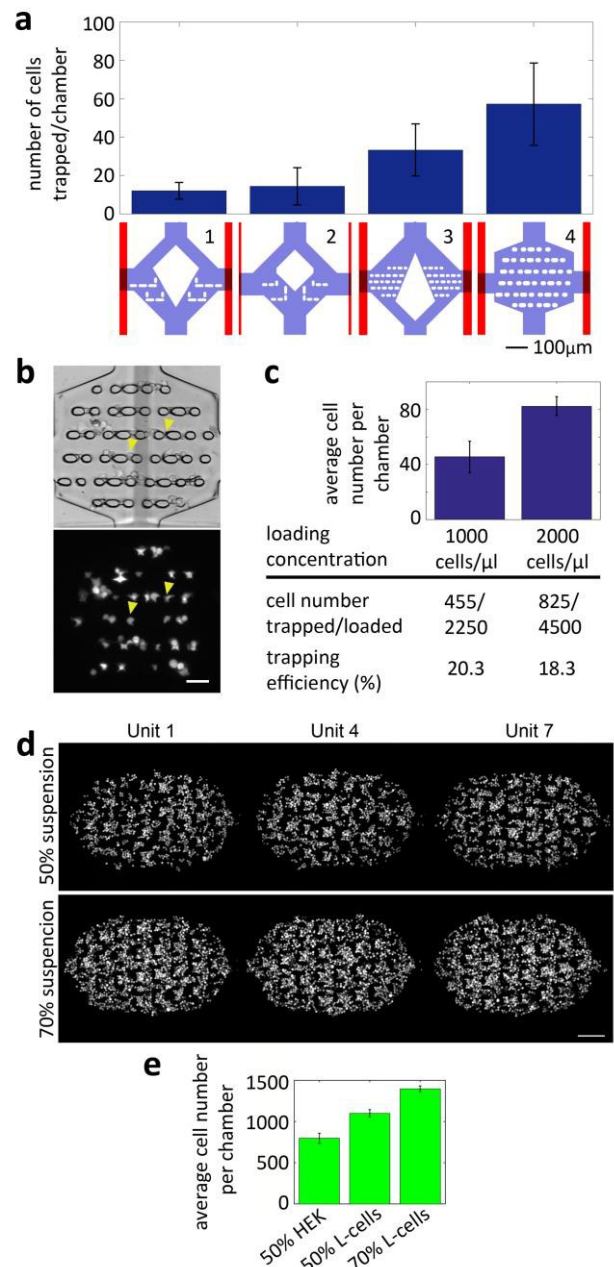


**Fig. 2** Trapping of rare stem cells and cell lines in the co-culture chemotaxis device. (a) Different designs of responder chambers were tested for maximal trapping of MSC. The best configuration (4<sup>th</sup> design) was then selected for the final chemotaxis setup. (n=3 experiments each; averages and standard deviations are displayed). (b) Bright field (top) and fluorescent (bottom) image of primary GFP<sup>+</sup> MSC in the responder chamber 15 minutes after loading. Yellow arrow heads exemplify two cells immobilized in the chamber by trapping pillars (Scale bar, 50 $\mu\text{m}$ ). (c) Trapping efficiency of small cell population of primary MSC. The efficiency was determined by comparing the total number of loaded with the total number of trapped cells per assay area of 10 basic units. (d) Fluorescent image of GFP<sup>+</sup> L-cells loaded into producer chambers. Three chambers are shown. The fluency in the chamber can be adjusted based on the concentration of the loading cell suspension (top and bottom row). Scale bar, 200 $\mu\text{m}$ . The total number of cells trapped per device depend also on the cell type (e, 50% to 70% cell suspension corresponds to concentration of 125'000 - 180'000 cells/ $\mu\text{L}$ ). Bars are means  $\pm$  s.d., n=10 units.

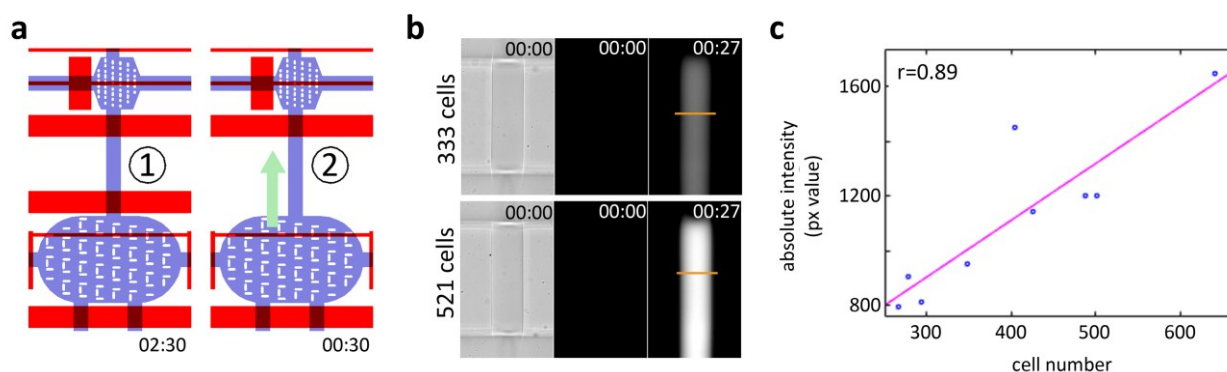


**Fig. 3** Secretion levels correspond to the number of loaded producer cells. (a) Schematic representation of the experimental design. After loading, cells were cultured for 2.5 h in the closed producer chambers, ①. The inner side valve was then opened and the protein was allowed to diffuse into the migration channel while the valve connecting the channel to the central responder chamber remained closed, ②. (b) Fluorescent imaging for individual units with either 333 or 521 cells was recorded at the start and at 27 min and quantified. The range for quantification is marked by an orange bar. (c) Correlation between the number of secNeonGreen<sup>+</sup> cells and the absolute fluorescent intensity in the migration channel ( $n=9$ ,  $p=0.00148$ ).

The producer chambers were loaded with cell lines and contained between 800 and 1400 cells per chamber depending on the cell type. The number of cells per chamber can be adjusted by altering the starting concentration of the cell suspension at loading (Fig. 2d, e). Due to a high loading concentration (125'000 cells/ $\mu\text{L}$  – 180'000 cells/ $\mu\text{L}$  for a 50% to 70% cells suspension), the loading of producer cells was very homogeneous. The loading time was kept as short as possible (up to 2min) to avoid differential stress on cells in a row of chambers<sup>29</sup> and formation of cell aggregates during seeding.<sup>30</sup>

#### On-chip protein production and formation of spatially and temporally stable concentration differences

We next wanted to measure if on-chip protein secretion is a linear function of the number of producer cells. In order to visualize protein secretion we generated a cell line that secretes a fluorescent protein (HEK293T cells stably expressing secNeonGreen, 28kDa). Different amounts of secNeonGreen<sup>+</sup> cells were loaded and cultured for 2.5 h in closed producer chambers. Afterwards, the inner side valve was opened and the protein was allowed to diffuse into the migration channel (Fig. 3a). At 27 min, we measured the maximal fluorescent intensity across the channel and observed a linear correlation ( $r = 0.89$ ,  $p=0.00148$ ,  $n=9$ ) between the number of producer cells and the absolute fluorescent intensity in the corresponding migration channel (Fig. 3b, c).

We next aimed to test whether protein production on-chip allows creating stable, long-lasting concentration differences in opposing migration channels and whether this difference is equal in all 10 units. We again used the secNeonGreen<sup>+</sup> cells (~600 cells per chamber) in order to visualize protein secretion and deduce protein concentration from fluorescent intensity measurements. We initially tried using flow-based gradient formation with our design; however, supplying the cells by continuous medium flow through the side channels resulted in flow through the migration channels (cross-unit flow, data not shown). Instead, we developed a “pulsed supply” method that

fed the cells by discontinuous medium replacement from reservoirs in the side channels. Automated cycles contained periods of medium flow in the side channels which were alternated with flow-free periods for medium replacement by diffusion. The scheme in Fig. 4a illustrates the steps of this cycle: 1) at end of the diffusion period the exchange between producer chambers and reservoirs was complete, 2) the side valves were closed and new medium was flown through side channels for 30 min, 3) afterwards, medium flow was stopped with valves at the inlet and outlet followed by opening the side valves for 30 min resulting in replenishing the producer chambers with fresh medium by diffusion. We abbreviated this cycle 30/30 (30 min flow / 30 min medium replacement by diffusion). Valves between individual producer or responder chambers were closed permanently to prevent cross-talk. Temporally separating medium flow and medium exchange prevented flow of liquid through the migration channels. The cells secreting chemoattractant create the pole with maximum concentration while constantly removing chemoattractant from the opposing side by the pulsed supply method creates a sink which maintains stable concentration gradients on opposing sides of the responder chamber (Fig. 4b). We measured fluorescent intensities in control and experimental migration channels in all ten units over 20 hours (Fig. 4c, e). When comparing all 10 units, the concentration differences were found to be very uniform with an average relative variation of 9 % between the units. Temporal stability was similar with relative variation of 9.15 % (Fig. 4d). Formation of stable gradients adding secNeonGreen-conditioned medium instead of on-chip production was possible as well (Supplementary Fig. 6a-c).

Since the concentration of secreted protein was reduced every time fresh medium was added to the producer cells, we tested different pulsed supply protocols. secNeonGreen<sup>+</sup> cells were fed by pulsed supply using either 10/5, 25/5 or 50/10 cycles so that the overall cycle duration was 15, 30 or 60 min. Fluorescent intensity measurements showed that concentration differences remained very similar,

independently of the overall duration of the cycle with an average relative variation between 7.5 to 8.6% (Fig. 4f).

### Chemotaxis of cells towards secreted chemokines

After we had optimized our system for long-term culture and generation of stable concentration differences for on-chip secreted proteins, we moved on to demonstrate the feasibility of our system for chemotaxis analysis. We made use of CXC chemokines which are known to control many aspects of cell migration during wound healing and immune system regulation.<sup>31</sup> We generated stable cell lines of CXCR3-expressing responder cells (R3 HEK, HEK293T transfected with a CXCR3 construct) and producer cells expressing the corresponding CXCL10 ligand (cells transfected with a CXCL10 construct; **Supplementary Fig. 7**). First we analysed the percentage of R3 HEK cells (relative to the total number of loaded cells in the unit) moving into the experimental (CXCL10) or the control (wt) migration channel. Already at the first time point (3h), we observed significantly more cells moving towards the CXCL10 cells ( $p < 0.0005$ ,  $n = 10$  positions analysed) and this preferential movement was increasing over time. The most significant difference in the number of migrating cells was observed at 12 h (Fig. 5a and b,  $p < 0.0000007$ ; **Supplementary Video 1**). In contrast, the same combination of cells used in classical transwell assays (Tr, Fig. 5b) exhibited a strongly (over 10 fold) reduced frequency of migrating cells. This indicated that long-term maintenance of gradients in the microfluidic device in contrast to the Boyden chamber allowed many more cells to migrate directionally. A further advantage of using a microfluidic device in combination with an automated microscope is that we can record the spatial dynamics of individual cells. We observed an increased average Y distance the responder cells were migrating towards the ligand-producing CXCL10 L-cells as compared to the control cells (Fig. 5c,  $p < 0.00003$  at 12 h). Responder cells moved preferentially towards CXCL10 independently of the number of responder cells that was loaded (**Supplementary Fig. 8a, b**). This directed migration towards CXCL10 was observed for up to 7 days (**Supplementary Fig. 8c, d**). In control experiments no significant differences in migration frequency or distance were observed when parental HEK293T cells (which do not express CXCR3) were tested against CXCL10<sup>+</sup> and control L-cells (Fig. 5d and e).

For primary MSC, no factors have been described to mediate chemoattraction. A number of factors (CXCL12, PDGF-B, CXCL16) had been reported to mediate attraction of in vitro expanded MSC.<sup>32-34</sup> However, these factors did not mediate chemoattraction of primary MSC in our hands (data not shown); possibly since the corresponding receptors were not sufficiently expressed on primary cells but were induced only after 2 weeks of in vitro culture (Abbuehl et al., manuscript submitted). We therefore generated CXCR3 expressing, primary MSC by lentiviral transduction (termed R3 MSC) 2 days after cell isolation (**Supplementary Fig. 7**) which was followed by chemotaxis assays at day 6. The fraction of R3 MSC migrating towards the chemokine was around 17 % with a

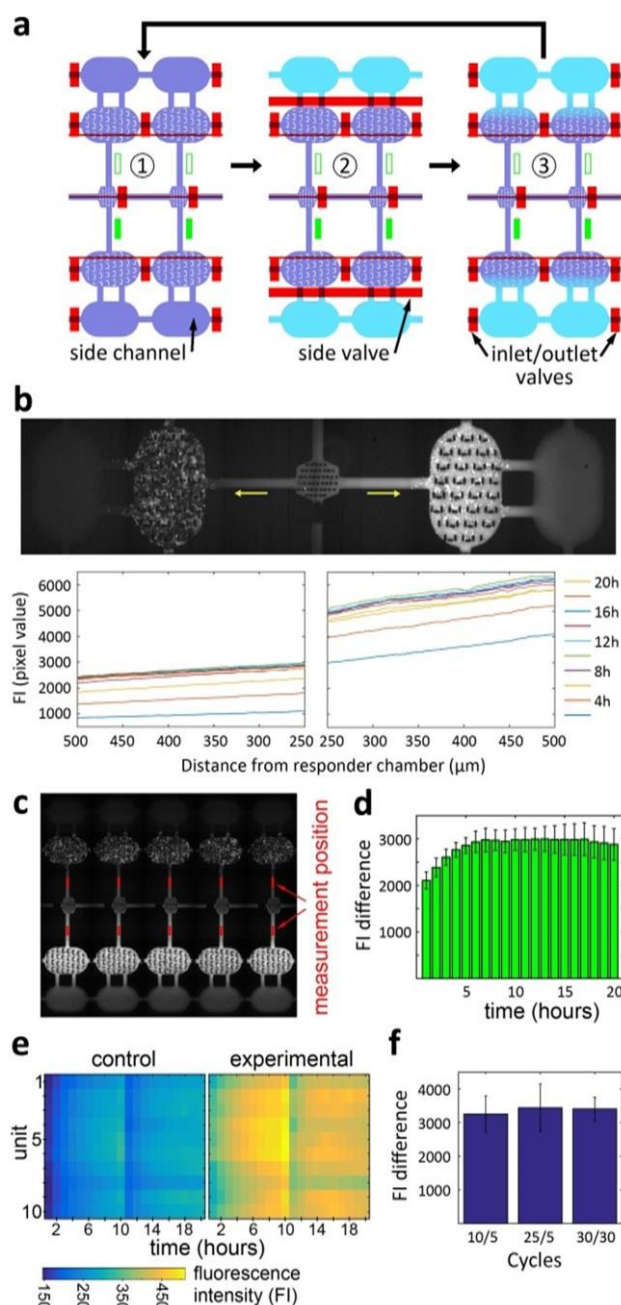


**Fig. 4** Stable concentration gradients formed with the pulsed supply method by on-chip secretion from secNeonGreen<sup>+</sup> cells. (a) Schematic presentation of pulsed supply cycles used for cell feeding and formation of stable concentration gradients on opposing sides of the responder chamber. (b) Fluorescent image of one basic unit with secNeonGreen<sup>+</sup> cells (right) and control GFP<sup>+</sup> HEK cells (left). Fluorescent intensity (FI) was measured in either migration channel at the given position (yellow arrow) over 20h (moving average filter with 10 μm window size). (c) Fluorescent image of 5 neighbouring units with secNeonGreen<sup>+</sup> cells in the bottom and control GFP<sup>+</sup> HEK cells in the top producer chambers 3h after the culture started. (d) Average difference in FI between experimental and control migration channels over all 10 units (mean and s.d. shown). (e) Mean fluorescent intensity (FI) was measured in control (top) and experimental (bottom) migration channels 250 μm from the responder chamber (area 60 x 250 μm, marked by red rectangles in c) and was plotted as heat map. Rows represent individual basic units while columns show evolution of FI over time with one central wash after 10 hours (absolute FI reduced due to changed light path). (f) Average FI difference with altered frequency of pulsed supply (means of 10 basic units with s.d.).

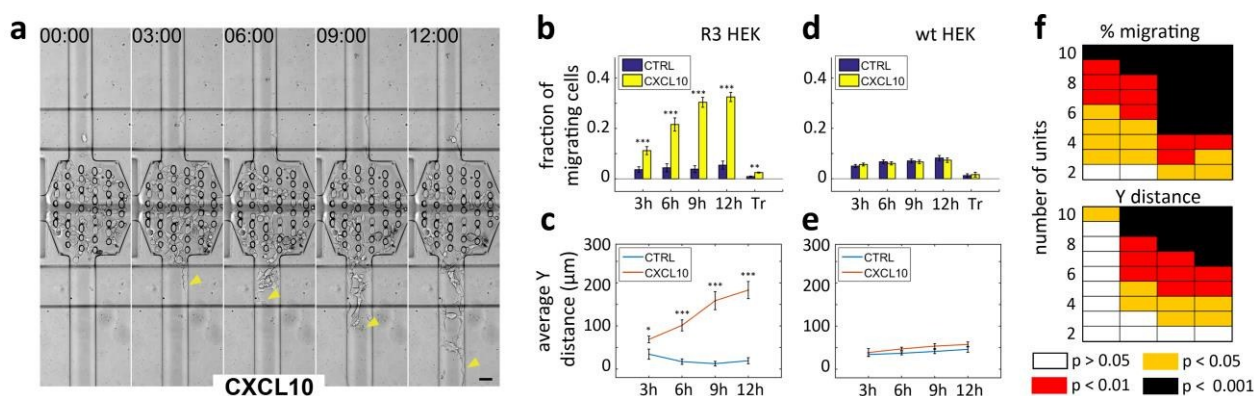


**Fig. 5** Functional validation of the co-culture chemotaxis design using CXCR3 HEK responder cells. **(a)** CXCR3<sup>+</sup> HEK293T (R3 HEK) cells were loaded to the responder chambers of the device while CXCL10-producing L-cells (CXCL10) were cultured in the bottom and control L-cells (CTRL) in the top producer chambers. After the R3 HEK cells adhered (time point 0 h, left image) co-culture was started and the migration potential of cells was analysed every 3 h for up to 12 h. Yellow arrow heads are pointing to the front responder cell moving into the experimental migration channel towards the chemokine. Producer chambers are not shown in the image sequence (Scale bar, 50 μm). **(b)** Number of cells moving into the migration channels towards CXCL10 or CTRL cells were normalized to the total number of responder cells to determine the fraction of migrating cells. On-chip experiments were compared to transwell assays (Tr, endpoint at 4.5h, n=3). **(c)** Average Y distance the R3 HEK cells had moved towards CXCL10 or CTRL cells was normalized to the total number of cells that moved out of the responder chamber. **(d, e)** Parental HEK cells transduced with the backbone construct (wt HEK) were used in control experiments. Values are mean ± s.e.m. (n=10); significance was calculated by a paired sample one-tailed t-test: \* p<0.05, \*\* p<0.01, \*\*\* p<0.001. **(f)** Jackknife resampling (delete-*m* observations) of the data shown in **b** (% of migrating cells) and **c** (Y distance) revealed that significant results were obtained from 2 or 3 basic units corresponding to 160 to 240 responder cells, respectively. Heatmap representation of the significance of the data using all possible combinations of 2-10 individual units as analysed by paired sample one-tailed t-test. Columns represent time points 3-12h.

maximal response at 15h compared to 7.7% of cells moving away from the chemokine (Fig. 6a;  $p < 0.0044$ ). Compared to R3 HEK, R3 MSC were slower to respond to the chemokine and showed significant chemoattraction only at 10 h (Fig. 6b,  $p < 0.024$ ). This demonstrates that extending assay duration is an important factor which allows analysing slowly responding cells such as this stem cell population. Further, the average Y distance these R3 MSC covered was significantly higher towards the chemokine than in the opposite direction (Fig. 6c; time point of maximal response at 15 h,  $p < 0.0011$ ). No preferential migration towards the chemokine was observed for wt MSC not expressing CXCR3 (Fig. 6c, d).

In order to determine the robustness of these chemotaxis assays, we performed Jackknife resampling (delete-*m* observations) of the data (Fig. 5f and 5e). This involved sequentially deleting an increasing number of units in all possible permutations and using the remaining data to determine the significance of the chemotactic response. This revealed that for both cell types, the most significant results were obtained at the 3rd time point (9h for HEK and 15h for MSC). While for the R3 HEK cells, already 3 units are sufficient to significantly measure preferential migration towards the chemokine, 4 units which corresponded to ~120 cells were required for primary mesenchymal stem cells. Being able to measure chemotaxis from only 120 primary stem cells testifies to the sensitivity of our platform as compared to the classical Boyden chamber assay which would require at least 80 times more cells for a single measurement without replicates. Taking advantage of the time-lapse video microscopy that was used to record individual cell positions over time we generated tracking data for analysis of additional migratory parameters (Fig. 6f, g). MSC were moving as single cells in contrast to R3

HEK cells that preferentially moved in sheets or clusters (Supplementary Video 1). We analysed speed (total migrated distance in any direction/time), velocity (net distance across the migration channel/time) and chemotaxis index (net distance across the migration channel / total distance) of the cells. Interestingly, for MSC none of these parameters were altered by the chemokine (data not shown) indicating that the chemoattractant largely acts to trigger migratory behaviour and to control directionality on top of an intrinsic propensity of these cells to move. In contrast, velocity and chemotaxis index were significantly enhanced for R3 HEK cells in response to the chemokine, while speed was not altered (Supplementary Fig. 9). Thus our platform allows not only to measure chemokine activity but also helps to identify alternative patterns of migratory behaviour in individual cell types.

## Discussion and Conclusions

Functional studies of tissue-specific stem cells are greatly impaired by dependence on their natural microenvironment and their sensitivity upon extraction.<sup>35,36</sup> Researchers thus often favour to perform assays with more robust cell types such as cell lines or stem cells adapted to in vitro culture by serial passaging. These cells are, however, phenotypically distinct from the tissue of origin and freshly isolated, primary cells should be preferred which better reflect the in vivo situation.<sup>37,38</sup> Recent development of microfluidic techniques enabled molecular characterization of rare stem cell populations with endpoint assays.<sup>39-41</sup> In contrast, functional characterization of stem cells with assays that study proliferation<sup>42,4</sup>, secretion<sup>5</sup>, or apoptosis<sup>43</sup> are still very challenging tasks. Such functional studies were performed

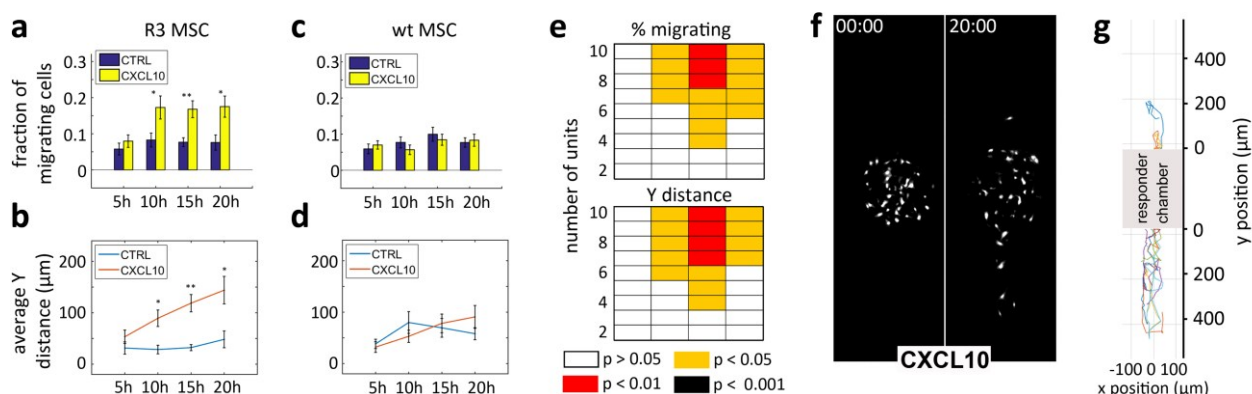


**Fig. 6** Chemotaxis of CXCR3<sup>+</sup> MSCs in our microfluidic device. Primary MSC were isolated from FVB/N mice, enriched by MACS and infected with a lentiviral vector for the simultaneous expression of mCherry and CXCR3. The CXCR3<sup>+</sup> mCherry<sup>+</sup> MSC (R3 MSC, ~300 positive cells) were analysed for their migration potential in co-culture with CXCL10-producing (CXCL10) and control (CTRL) L-cells. (a) The fraction of MCS responders moving into the migration channels towards CXCL10 (top) or ctrl (bottom) producer cells at different time points was determined relative to the total number of loaded R3 MSC responder cells. (b) Average Y distance that the R3 MSC responder cells had moved at a given time point was normalized to the total number of cells that moved out of the responder chamber. (c, d) MSC cells transduced with the backbone construct (wt MSC) were used in control experiment. Values are mean + s.e.m. (n=10); significance was calculated by a paired sample one-tailed t-test; \* p<0.05, \*\* p<0.01, \*\*\* p<0.001. (e) Jackknife resampling (delete-m observations) of the data shown in a (% of migrating cells) and b (Y distance) revealed that significant results were obtained from 4 units corresponding to 120 R3 MSC responder cells. Heatmap representation of the significance of the data using all possible combinations of 2-10 individual units as analysed by paired sample one-tailed t-test. Columns represent time points 5-20h. (f) Representative fluorescent image of CXCR3<sup>+</sup> MSC on-chip at loading (left) or after 20h (right) of chemoattraction by CXCL10 producer cells (bottom) vs. CTRL cells (top; producer chambers not shown). (g) Tracking of individual CXCR3<sup>+</sup> MSC (each coloured line represents x/y positions of one cell) by time-lapse (30 min interval) microscopy over 20 h. Responder chamber part is masked.

mainly with hematopoietic progenitor cells which can be obtained in higher number.

We focused on mesenchymal stem cells which have been reported to migrate from the bone marrow to tumor sites where they promote cancer progression.<sup>44,34</sup> Mesenchymal stem cells are rare and typically only 10000 cells can be obtained from one mouse. Chemotaxis is classically studied *in vitro* by the use of transwell migration assays which, however, are inherently limited: 1) the created gradient is only of transient nature which limits analysis to fast responding and fast migrating cells; 2) each assay requires at least 10000 cells per condition which restricts analysis to abundant cell types. We therefore decided to develop a microfluidic device to study the chemotaxis of rare, primary, bone marrow derived MSC. In order to be able to quantify results and to test several factors in parallel in the future, the device was compartmentalized into separate, identical basic units. This resulted in nanoliter-size chambers for the culture of MSC which were much smaller than previously described microfluidic devices.<sup>14-16</sup> Long-term cell culture in such small chambers required a number of optimizations (**Supplementary Table 1**) which only in combination allowed performing chemotaxis assays with primary MSC.

Hydrodynamic trapping has been previously described to be highly efficient for immobilization of cells in microfluidic devices.<sup>28,27,45</sup> However, the low number of primary MSC posed a second major problem and required to optimize cell traps in order to at the same time maximize yield from input material and distribute cells equally between basic units. To produce trapping structures we were inspired by a study from the Thorsen lab.<sup>27</sup> We introduced similar U-shaped traps

which resulted in very equal trapping of cell lines in our producer chambers with little variation between units. However, these structures resulted in extensive cell loss when used for small and diluted MSC samples. Thus we decided to use more compact trapping structures consisting of rows of pillars (**Fig.2** and **Supplementary Figure 1**) which resulted in even distribution throughout each chamber and equal loading over all units. The achieved trapping efficiency was ~20% from the input material. A recent study used densely spaced, single-cell traps and accomplished ~80% trapping efficiency.<sup>46</sup> However, these traps have a large footprint per cell decreasing the efficiency of the chemotaxis assay, since cells have to reach the migration channels fast enough which limits the size of the responder chamber.

We decided to use on-chip protein secretion from mammalian cells for highest biological activity of the produced factors.<sup>47-49,12</sup> Mammalian cells can easily surpass microbial systems for the production of secreted proteins due to the need for correctly processed and folded proteins with often complex post-translational modifications. In contrast, many bacterially-produced proteins have to be re-folded from inclusion bodies which often results in preparations of uncertain quality and biological activity. One additional benefit of protein production within the microfluidic device is the ability to obtain higher cell densities in relation to culture volume. While the (packed) volume of cells in large-scale, bio-reactor cultures typically correspond to only 2–3% of the total volume, microbial cultures can achieve a packed cell volume of 30% or more. With a cell volume of 10-20% (relative to the chamber volume), our microfluidic device gets close to the microbial conditions with the added value of mammalian processing and

glycosylation. In this study we introduced a novel secreted NeonGreen fluorescent reporter that helped us visualizing temporal and spatial stability of the produced gradients. It further allowed comparing protein concentrations produced on-chip vs. production in standard cultures as conditioned medium: on-chip production reaches ~7 times higher concentrations as determined by FI measurements (Fig. 4b vs. Supplementary Fig. 6a) likely due to the increased cell density. On-chip protein production required discontinuous medium exchange to facilitate stable gradient formation; we therefore developed a pulsed supply method. This contributed to extending assay duration for up to 7 days while maintaining cell viability and directional cell migration (**Supplementary Fig. 8**). Prolonging assay duration can help to counteract the random migratory propensity of cells which show delayed responses to the chemokine gradient and adapt their direction of movement only later (**Supplementary Fig. 8c**; compare 12h and later time points). Even though not designed for this purpose, the device can also be used for chemotaxis assays with defined, externally added factors or to isolate responder cells for further downstream assays (**Supplementary Fig. 10, 11**).

We conclude that our microfluidic device allows for the first time to perform chemotaxis measurements for primary stem cells in response to defined attractors. The strongly reduced volumes in this device and the automated control of fluidics allow forming long-term stable protein gradients from few producer cells by on-chip protein secretion. This prolonged assay duration resulting in a strikingly increased number of migrating cells which is essential for analysing rare or slowly responding cell populations. This new device can provide the basis for developing a high-throughput platform for the analysis of a number of primary stem cells. It will be straightforward to combine on-chip reverse transfection with on-chip protein production in order to form an array of producer chambers producing a larger set of secreted proteins. Our device can easily be further multiplexed to include more basic units so that arrays of up to 200 different proteins per device can be assayed at once. This will allow to systematically test chemotaxis towards a given set of chemoattractants and to facilitate analysis of a number of migration characteristics of individual cells. This will significantly add to our understanding of how migration of stem cells is regulated.

## Acknowledgements

Z.T., S.M. and J.H. were supported in part by grants from the SNF. We thank Paloma Ordóñez-Morán for generating CXCL10 expressing L cells, Samuel Gex for constructing the device holder and Pierre Dessen for the generation of lentiviral constructs. The authors declare that they do not have a conflict of interest.

## Notes and references

- 1 M. J. Kiel, O. H. Yilmaz, T. Iwashita, C. Terhorst and S. J. Morrison, *Cell*, 2005, **121**, 1109-1121.
- 2 N. Barker, J. H. van Es, J. Kuipers, P. Kujala, B. M. van den, M. Cozijnsen, A. Haegebarth, J. Korving, H. Begthel, P. J. Peters and H. Clevers, *Nature.*, 2007, **449(7165)**, 1003-1007.
- 3 B. O. Zhou, R. Yue, M. M. Murphy, J. G. Peyer and S. J. Morrison, *Cell Stem Cell*, 2014, **15**, 154-168.
- 4 V. Lecault, M. Vaninsberghe, S. Sekulovic, D. J. Knapp, S. Wohrer, W. Bowden, F. Viel, T. McLaughlin, A. Jarandehi, M. Miller, D. Falconnet, A. K. White, D. G. Kent, M. R. Copley, F. Taghipour, C. J. Eaves, R. K. Humphries, J. M. Piret and C. L. Hansen, *Nat Methods*, 2011, **8**, 581-586.
- 5 J. L. Zhao, C. Ma, R. M. O'Connell, A. Mehta, R. DiLoreto, J. R. Heath and D. Baltimore, *Cell Stem Cell*, 2014, **14**, 445-459.
- 6 C. Ma, R. Fan, H. Ahmad, Q. Shi, B. Comin-Anduix, T. Chodon, R. C. Koya, C. C. Liu, G. A. Kwong, C. G. Radu, A. Ribas and J. R. Heath, *Nat Med*, 2011, **17**, 738-743.
- 7 D. J. Prockop, *Mol Ther*, 2009, **17**, 939-946.
- 8 A. Peled, I. Petit, O. Kollet, M. Magid, T. Ponomaryov, T. Byk, A. Nagler, H. Ben-Hur, A. Many, L. Shultz, O. Lider, R. Alon, D. Zipori and T. Lapidot, *Science*, 1999, **283**, 845-848.
- 9 S. B. Asokan, H. E. Johnson, A. Rahman, S. J. King, J. D. Rotty, I. P. Lebedeva, J. M. Haugh and J. E. Bear, *Developmental Cell*, 2014, **31**, 747-760.
- 10 S. Boyden, *J Exp Med*, 1962, **115**, 453-466.
- 11 J. Li and F. Lin, *Trends Cell Biol*, 2011, **21**, 489-497.
- 12 I. K. Zervantonakis, C. R. Kothapalli, S. Chung, R. Sudo and R. D. Kamm, *Biomicrofluidics*, 2011, **5**, 13406.
- 13 P. Ertl, D. Sticker, V. Charwat, C. Kasper and G. Lepperdinger, *Trends Biotechnol*, 2014, **32**, 245-253.
- 14 V. V. Abhyankar, M. A. Lokuta, A. Huttenlocher and D. J. Beebe, *Lab Chip*, 2006, **6**, 389-393.
- 15 S. K. Dertinger, X. Jiang, Z. Li, V. N. Murthy and G. M. Whitesides, *PNAS*, 2002, **99**, 12542-12547.
- 16 T. M. Keenan, C. W. Frevert, A. Wu, V. Wong and A. Folch, *Lab Chip*, 2010, **10**, 116-122.
- 17 J. R. Rettig and A. Folch, *Analytical Chemistry*, 2005, **77**, 5628-5634.
- 18 N. Ferrell, D. Gallego-Perez, N. Higuera-Castro, R. T. Butler, R. K. Reen, K. J. Gooch and D. J. Hansford, *Analytical Chemistry*, 2010, **82**, 2380-2386.
- 19 W. H. Tan and S. Takeuchi, *PNAS*, 2007, **104**, 1146-1151.
- 20 L. Lin, Y. S. Chu, J. P. Thiery, C. T. Lim and I. Rodriguez, *Lab Chip*, 2013, **13**, 714-721.
- 21 H. Wang, F. Cao, A. De, Y. Cao, C. Contag, S. S. Gambhir, J. C. Wu and X. Chen, *Stem Cells*, 2009, **27**, 1548-1558.
- 22 N. C. Shaner, G. G. Lambert, A. Chammas, Y. Ni, P. J. Cranfill, M. A. Baird, B. R. Sell, J. R. Allen, R. N. Day, M. Israelsson, M. W. Davidson and J. Wang, *Nat Methods*, 2013, **10**, 407-409.
- 23 Y. S. Heo, L. M. Cabrera, J. W. Song, N. Futai, Y. C. Tung, G. D. Smith and S. Takayama, *Analytical Chemistry*, 2007, **79**, 1126-1134.

- 24 C. A. Schneider, W. S. Rasband and K. W. Eliceiri, *Nat Methods*, 2012, **9**, 671-675.
- 25 M. Matasci, D. L. Hacker, L. Baldi and F. M. Wurm, *Drug Discov Today Technol*, 2008, **5**, e37-42.
- 26 C. Luni, E. Serena and N. Elvassore, *Curr Opin Biotechnol*, 2014, **25**, 45-50.
- 27 Z. Wang, M. C. Kim, M. Marquez and T. Thorsen, *Lab Chip*, 2007, **7**, 740-745.
- 28 D. Di Carlo, L. Y. Wu and L. P. Lee, *Lab Chip*, 2006, **6**, 1445-1449.
- 29 X. Xu, Z. Li and A. Nehorai, *Biomicrofluidics*, 2013, **7**, 54108.
- 30 Z. Wang, M. C. Kim and T. Thorsen, *Ann Int Conf IEEE Engin Med Biol Soc*, 2008, **2008**, 2752-2755.
- 31 R. Gillitzer and M. Goebeler, *Journal of Leukocyte Biology*, 2001, **69**, 513-521.
- 32 A. L. Ponte, E. Marais, N. Gallay, A. Langonne, B. Delorme, O. Herault, P. Charbord and J. Domenech, *Stem Cells*, 2007, **25**, 1737-1745.
- 33 M. Iannone, M. Ventre, G. Pagano, P. Giannoni, R. Quarto and P. A. Netti, *Biotechnology and Bioengineering*, 2014, **111**, 2303-2316.
- 34 Y. Jung, J. K. Kim, Y. Shiozawa, J. Wang, A. Mishra, J. Joseph, J. E. Berry, S. McGee, E. Lee, H. Sun, T. Jin, H. Zhang, J. Dai, P. H. Krebsbach, E. T. Keller, K. J. Pienta and R. S. Taichman, *Nat Commun*, 2013, **4**, 1795.
- 35 B. P. Mahadik, S. Pedron Haba, L. J. Skertich and B. A. Harley, *Biomaterials*, 2015, **67**, 297-307.
- 36 W. S. Hong, E. W. Young, W. H. Tepp, E. A. Johnson and D. J. Beebe, *Toxicol Sci*, 2013, **134**, 64-72.
- 37 C. Pan, C. Kumar, S. Bohl, U. Klingmueller and M. Mann, *Mol Cell Proteomics*, 2009, **8**, 443-450.
- 38 C. S. Alge, S. M. Hauck, S. G. Priglinger, A. Kampik and M. Ueffing, *Journal of proteome research*, 2006, **5**, 862-878.
- 39 A. M. Klein, L. Mazutis, I. Akartuna, N. Tallapragada, A. Veres, V. Li, L. Peshkin, D. A. Weitz and M. W. Kirschner, *Cell*, 2015, **161**, 1187-1201.
- 40 J. F. Zhong, Y. Chen, J. S. Marcus, A. Scherer, S. R. Quake, C. R. Taylor and L. P. Weiner, *Lab Chip*, 2008, **8**, 68-74.
- 41 A. M. Streets, X. Zhang, C. Cao, Y. Pang, X. Wu, L. Xiong, L. Yang, Y. Fu, L. Zhao, F. Tang and Y. Huang, *PNAS*, 2014, **111**, 7048-7053.
- 42 T. Cambier, T. Honegger, V. Vanneaux, J. Berthier, D. Peyrade, L. Blanchoin, J. Larghero and M. They, *Lab Chip*, 2015, **15**, 77-85.
- 43 S. L. Faley, M. Copland, D. Wlodkowic, W. Kolch, K. T. Seale, J. P. Wikswo and J. M. Cooper, *Lab Chip*, 2009, **9**, 2659-2664.
- 44 A. E. Karnoub, A. B. Dash, A. P. Vo, A. Sullivan, M. W. Brooks, G. W. Bell, A. L. Richardson, K. Polyak, R. Tubo and R. A. Weinberg, *Nature*, 2007, **449**, 557-563.
- 45 A. Lawrenz, F. Nason and J. J. Cooper-White, *Biomicrofluidics*, 2012, **6**, 24112-2411217.
- 46 B. Dura, S. K. Dougan, M. Barisa, M. M. Hoehl, C. T. Lo, H. L. Ploegh and J. Voldman, *Nat Commun*, 2015, **6**, 5940.
- 47 Y. S. Torisawa, B. Mosadegh, T. Bersano-Begey, J. M. Steele, K. E. Luker, G. D. Luker and S. Takayama, *Integr Biol (Camb)*, 2010, **2**, 680-686.
- 48 S. L. Chang, S. P. Cavnar, S. Takayama, G. D. Luker and J. J. Linderman, *PLoS One*, 2015, **10**, e0123450.
- 49 S. Chung, R. Sudo, P. J. Mack, C. R. Wan, V. Vickerman and R. D. Kamm, *Lab Chip*, 2009, **9**, 269-275.